Proceedings of Global Power and Propulsion Society
ISSN-Nr: 2504-4400
GPPS Montreal26
September 9-11, 2026
www.gpps.global

GPPS-TC-2026-0022

Optimization of the volute of a supersonic organic Rankine cycle radial-inflow turbine

Yannik Schulz[1,3,*], Francesco Vaccari[2,3,*], Matteo Pini[2,3], Dajan Mimic[1,3]
[1]**Institute of Turbomachinery and Fluid Dynamics, Leibniz University Hannover**
[2]**TU Delft, Faculty of Aerospace Engineering – Propulsion and Power**
[3]**Cluster of Excellence SE²A – Sustainable and Energy Efficient Aviation, TU Braunschweig**
*y.schulz@tfd.uni-hannover.de
Garbsen, Germany
*f.vaccari@tudelft.nl
Delft, The Netherlands

ABSTRACT

Organic Rankine cycle (ORC) power systems can efficiently utilize low- to medium-temperature heat sources, thus representing a viable technology for waste-heat recovery from prime engines. Radial-inflow turbines are a common choice for ORC expanders in systems with a power capacity in the range 10-200 kW, thanks to their compactness, simplicity, and high efficiency. These machines operate partially in non-ideal compressible flow regimes. Their aerodynamic design requires the use of specialized methods, which must take into account the occurrence of non-ideal thermodynamic states of the working fluid.

One of the components of such a turbo-expander is the volute, which has the role of distributing the flow circumferentially to the stator nozzles. This research work aims to investigate the flow within the volute of an ORC turbine with numerical simulations: the ORCHID turbine is a 10 kW, high-speed, single-stage radial-inflow turbine operating with hexamethyldisiloxane (siloxane MM) as the working fluid, under realization at the Aerospace Propulsion and Power laboratory of Delft University of Technology.

First, conventional design methods based on a 1D flow analysis with a free-vortex flow assumption are applied to design the volute. Two volute designs, obtained under the assumption of constant angular momentum and circumferentially uniform flow, are evaluated. Secondly, a CFD-based shape design of the volute using a genetic algorithm is performed by optimizing the passage area distribution. Finally, based on the attained optimal geometry, new best practices for the design of the volute in supersonic radial-inflow ORC turbines are formulated.

INTRODUCTION

Under the Paris Climate Agreement, 196 countries committed to limiting the increase in the global average temperature to 2 °C above pre-industrial levels, while pursuing efforts to keep it below 1.5 °C (Agreement, 2015). Achieving these targets requires substantial reductions in carbon dioxide (CO_2) emissions, both through the transition to renewable energy sources and by improving the efficiency of conventional systems. According to Cullen and Allwood (2010), the conversion efficiency of fossil primary energy into electricity is approximately 32%, while aircraft engines operate at around 25% efficiency. In both cases, the majority of the remaining energy is dispersed as waste heat. Consequently, recovering this waste heat represents a promising pathway for emission reductions, for instance, by utilizing it in Organic Rankine Cycle (ORC) systems. ORC technology is analogous to the conventional steam Rankine cycle but employs organic working fluids—such as refrigerants or hydrocarbons—allowing the effective exploitation of low- to medium-temperature heat sources (Rahbar et al., 2017). Typically, turbomachinery expanders, such as radial- or axial-inflow turbines, are preferred due to their superior efficiency (Pethurajan et al., 2018). For small-scale applications, the radial-inflow turbine is particularly attractive, as it is less sensitive to blade-profile tolerance issues and tip clearance losses when compared to axial-inflow turbines, and requires fewer blades per stage, offering cost benefits (Rahbar et al., 2017).

When considering radial-inflow turbines, the upstream volute is a crucial component that provides the inflow to the stator vanes. The area distribution over the circumference of volutes for conventional turbines is usually designed by either

This work is licensed under **Attribution-NonCommercial-NoDerivatives 4.0 International (CC-BY-NC-ND)**
See: https://creativecommons.org/licenses/by-nc-nd/4.0/legalcode

assuming one-dimensional incompressible flow and a free vortex distribution, see e.g. Shah et al. (2014), or one-dimensional incompressible flow and constant angular momentum, see e.g. Ebaid et al. (2003). In addition, volute performance is influenced by the choice of the cross-sectional shape and the volute tongue. Regarding the volute tongue Suhrmann et al. (2012) found that a small tongue angle paired with a small tongue radius achieve the best performance. The influence of the cross-sectional shape was studied by Qiang et al. (2010). They showed that a backward-installed volute of circular shape with an asymmetric outlet delivers the most uniform outflow when compared to symmetric or forward-facing asymmetric volutes.

ORC applications, however, can differ drastically when compared to conventional ones. The volute is generally followed by stator vanes, in which the flow can be choked and which can discharge supersonically. Moreover, in such machines, the behavior of the working fluid can be non-ideal (De Servi et al., 2019). Still, the conventional design methods are applied for designing ORC turbine volutes, see e.g. Filali and Semmari (2025), if the volute is considered at all. To the knowledge of the authors, no optimization has been conducted on ORC turbine volutes, and consequently, the quality of the conventional design methods cannot be assessed.

Research context and motivation

The Organic Rankine Cycle Hybrid Integrated Device (ORCHID) is a *hexamethyldisiloxane* (MM) closed-loop facility situated at TU Delft, designed to house both a nozzle section for fundamental non-ideal compressible fluid dynamics (NICFD) studies and a separate loop for testing a turbine operating partially in non-ideal conditions (Head, 2021).

The facility has been used previously for fundamental gas-dynamic studies on nozzle flows (Beltrame et al., 2021) and optical measurement techniques (Michelis et al., 2024), while the turbine loop is in its final phases of commissioning and scheduled to begin its measurement campaigns in 2026.

The machine is a compact, high-speed (100,000 rpm), high expansion ratio (>40) radial-inflow turbine (RIT) with a supersonic (Ma>2) stator outlet flow, see Majer et al. (2025). Experiments on such a turbine have the goal of providing open experimental data for the validation of numerical tools as well as the development of design practices for unconventional turbomachinery.

Detailed information on the design process of the turbine can be found in Majer (2025), where the preliminary design methodology and the detailed design of the laboratory test rig are described. In particular, the volute was manufactured by an external supplier by adapting an existing design to connect to the test bench infrastructure.

In the development of the ORCHID turbine, no CFD validation of either the volute as an isolated component or its interaction with the rest of the system was carried out; therefore, the design relied solely on reduced-order modeling, without validation or optimization using higher-fidelity tools.

Therefore, this work sets out to quantify the influence of the volute passage area distribution on the performance of an ORC turbine by means of optimization, to determine the optimal tongue position, to explore the accuracy of reduced-order design methods, which are based on conventional fluids, and finally, to provide design recommendations.

These goals are achieved by first carrying out a CFD-based genetic optimization at the design point. Afterwards, the optimized volute, the baseline, and two conventionally designed volutes are simulated at on- and off-design conditions using a full-annulus turbine model, and their performance, as well as the underlying flowfields, are evaluated in detail.

METHODOLOGY

Conventional volute design methods

The established boundary conditions that drive the volute design are given by the stator height b_1, the stator inlet radius r_1, the stator inlet metal angle β_g, total conditions at the volute inlet, and the mass flow rate, and are summarized in Tab. 1.

Table 1 Volute design boundary conditions

Parameter	b_1	r_1	β_g	$p_{t,1}$	$T_{t,1}$	$\dot{m}$
Value	2 mm	37.5 mm	65°	18.1 bar	573.15 K	0.132 kgs^{-1}

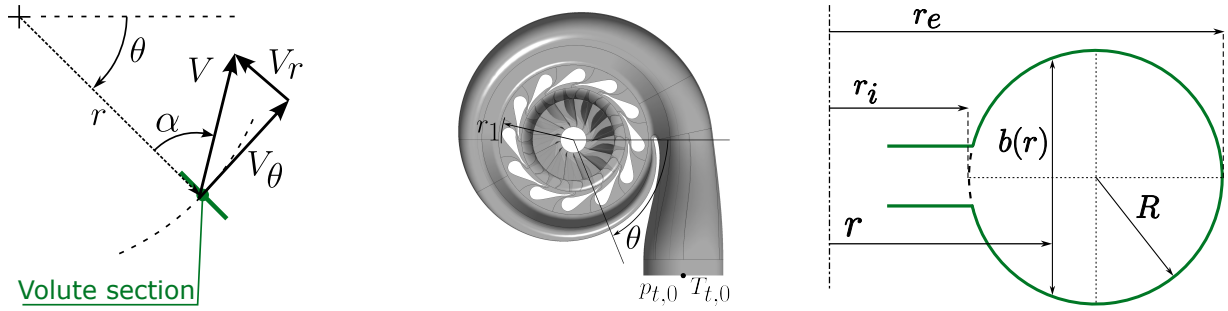
Assuming a uniform distribution of mass flow rate at the stator inlet and writing the conservation of mass on any volute cross-section along the tangential coordinate θ, yields:

$$\dot{m}\frac{\theta}{2\pi} = \int_{r_i}^{r_e} \rho V_\theta b(r) dr \tag{1}$$

where the velocities are defined according to the convention shown in Fig. 1a, the locations of the boundary conditions are given in Fig. 1b, and r_i and r_e are the inner and outer radii of the cross section of the volute, respectively, as defined in Fig. 1c.

This equation can be solved by using simplifying assumptions in order to design the volute area distribution. The simplest design methods rely on the assumption of incompressible flow. Two conventional design methods were investigated: one assuming constant tangential discharge velocity V_θ, the other assuming a free vortex distribution. An additional

assumption is that the inner radius is approximately equal to the stator inlet radius $r_i \approx r_1$, removing from the integral the section of the volute with parallel walls.



(a) Radial coordinates (b) Actual design (c) Cross-section

Figure 1 Nomenclature for volute quantities

For this set of boundary conditions, the radial velocity component $V_{r,1}$ is fully determined by mass conservation, and since the stator inlet angle is also defined, $V_{\theta,1} = V_{r,1} \tan \alpha_1$ is fully determined.

The first method by Stepanoff (1957) assumes constant tangential velocity V_θ at every section, the radius distribution for a circular cross-section becomes:

$$\pi R^2(\theta) = \frac{Q}{V_{\theta,1}} \frac{\theta}{2\pi} \Rightarrow R(\theta) = \sqrt{\frac{\theta Q}{2\pi^2 V_{\theta,1}}} \tag{2}$$

where $Q = \dot{m}/\rho$ is the total volumetric flow rate through the machine.

Another popular design method is obtained by imposing constant angular momentum $rV_\theta = \text{const.}$ between the centroid of any volute section and the stator inlet, effectively imposing a free vortex velocity distribution. By solving Eq. (1) for a circular cross-section, see e.g.: Fister (1986), the radius distribution over the circumference can be obtained:

$$R(\theta) = \frac{\theta Q}{4\pi^2 r_1 V_{\theta,1}} + \sqrt{\frac{\theta Q}{2\pi^2 V_{\theta,1}}} \tag{3}$$

A comparison of the two designs with the area distribution for the manufactured volute is shown in Fig. 2. The existing volute design has a significantly larger passage compared to the other two: given the very compact size of the machine, the choice of the inlet diameter was constrained mainly by a requirement of larger inlet tubing (⌀40mm) upstream of the turbine, to avoid excessive velocities in some of the flow control components. For this reason, during the optimization process, the inlet area of the volute was kept constant and equal to the manufactured one. The cross-sectional shape of the manufactured volute was provided by the original equipment manufacturer, adapted to match the tubing diameter at the inlet section and a linear area distribution.

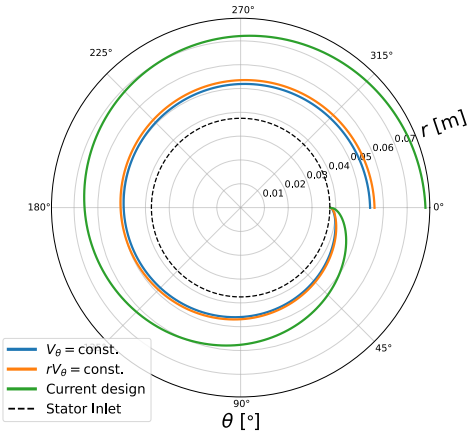


Figure 2 Outer volute radius for Conventional designs versus the current volute design

Parametric model setup

A parametric version of the original volute model was not available; thus, a modified version with overhung circular cross-sections was designed, shown schematically in Fig. 3. This design was chosen for its simplicity, ease of parametrization, and applicability of the design methods just described directly to the cross-sectional radius.

The implicit assumption in this treatment is that, although the shape might need to be adjusted in an actual design for manufacturing and mechanical reasons, information on an optimal area distribution to improve machine performance will carry over to a generic volute shape.

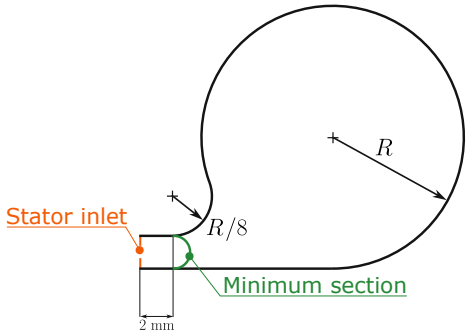
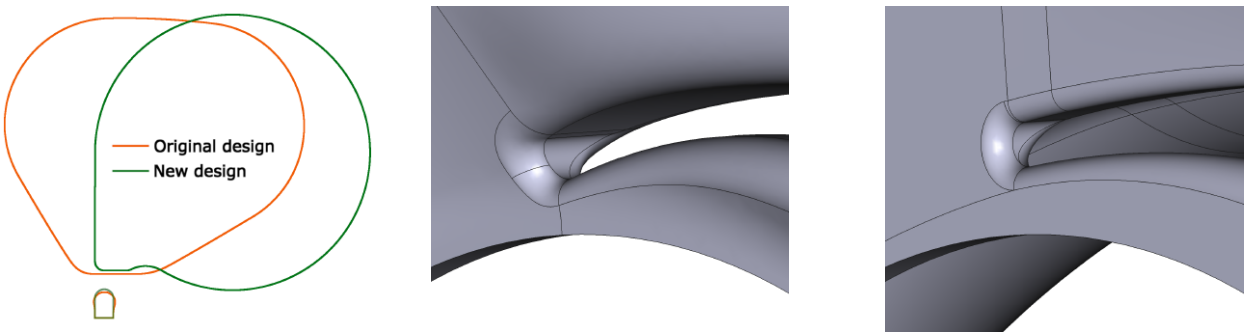


Figure 3 New design for volute cross-section geometry

Modifying the cross section also causes the tongue geometry to change; under this aspect, an effort was made to preserve the topology of the tongue as closely as possible to the original volute to ensure comparability. The tongue radius was also matched to the original and kept constant during the optimization procedure; details on the changes to its geometry are shown in Fig. 4.



(a) Cross-section comparison **(b) Original design, 3D view** **(c) New design, 3D view**

Figure 4 Tongue geometry comparison

Numerical model

All simulations in this work utilize the RANS CFD solver ANSYS CFX2024.2 (ANSYS, 2024*a*), using the high resolution scheme (a bounded second-order upwind biased discretization) for both advection and turbulence. Turbulence is modeled using the SST turbulence model (Menter et al., 2003), which provided a good match to the experimental data of an ORC turbine in terms of power, while the efficiency matched well for all but the operating point at the highest total inlet pressure (Seume et al., 2017). Transition is accounted for by the $\gamma - \mathrm{Re}_\theta$ transition model (Menter et al., 2006). The transition model was chosen as it is expected to improve the flow field prediction, since Oliveti et al. (2020) showed the accurate prediction of the transition location for the supersonic flow over a flat plate using the working fluid siloxane when compared to DNS data. In addition, the Kato-Launder production limiter (Kato, 1993) is used to fix the stagnation point anomaly. The working fluid MM is treated as a non-ideal gas and working fluid properties are obtained by means of a lookup table, generated from Fluidprop (Colonna et al., 2004), using the Span-Wagner equation for thermodynamic properties (Span and Wagner, 2003) and the Chung model for transport property values (Chung et al., 1988). Total inlet pressure (18.1 bar at design point) and temperature (573 K) boundary conditions are imposed at the inlet, while a static pressure boundary condition of 44,100 Pa is used at the outlet. All walls are treated as adiabatic.

Based on the aforementioned test case, three different simulation models are derived. The first model comprises the volute, single channels for both stator and rotor, and a diffuser segment, all connected via mixing planes. ANSYS Turbogrid is used to generate structured meshes of the rotor and stator, while ANSYS Mesh is utilized to generate unstructured

tetra/prism meshes of the volute and the diffuser. To ensure a resolution of the boundary layer, y^+ is kept below 2. The spatial independence is evaluated using the method of Roache (1998) based on the baseline volute. The mixing plane setup was used because a full annulus study was not feasible computationally. The study was performed at the design point using a refinement rate of 1.5 with respect to the mass flow rate. The errors in terms of the grid convergence index (GCI), which can be understood as an error band for the chosen resolution, and the extrapolated estimated relative error (EERE), which is the difference of the simulated value to the Richardson extrapolated, asymptotic value, are summarized in Tab. 2. The medium resolution was chosen as it showed spatial independence.

Table 2 Grid indepence study

Refinement	**Number of nodes**	**Mass flow rate in kg/s**	**GCI**	**EERE**
Coarse	2,466,852	0.13235	0.0027	0.0022
Medium	4,324,790	0.13215	0.0008	0.0006
Fine	10,533,260	0.13208	0.0001	0.0001

To resolve the effect of the volute tongue, but limit the computational effort during the optimization, the second numerical model consists of the volute, a full-annulus stator, and a singular rotor passage. The volute and stator are connected via a general connection interface, while the stator and rotor are connected by a mixing plane. The static pressure at the rotor outlet was determined from a simulation of the single-passage setup as 40,000 Pa. The optimization setup consists of around 16,100,000 nodes.

To examine the influence of the differently designed volutes (baseline, free vortex, constant tangential velocity, optimized) on the turbine performance in detail, a full-annulus model consisting of volute, stator, rotor, and diffuser was built. The clocking angle between volute and stator is set according to the optimization results for all configurations. The full-annulus setup consists of 48,500,000 nodes. The investigated operating points are summarized in Tab. 3. Under design conditions, the Reynolds number with respect to the volute inlet diameter and the volute inlet conditions is 342,000, while the one with respect to the stator chord and stator inlet conditions is 800,000, and $4.4 \cdot 10^6$ with respect to the stator outlet conditions.

Table 3 Operating point matrix

$p_{t,0}$ in bar: / Rotational speed in rpm:	10.9	14.5	18.1	23.5
80,000	OP1	OP4	OP7	OP9
98,100	OP2	OP5	**DP**	OP10
120,000	OP3	OP6	OP8	OP11

The accuracy of the different simulation models and the transition model is assessed by simulating the transitional mixing plane setup and the transitional and fully turbulent full-annulus models at the design point. The results in terms of mass flow rate, total-to-static machine and rotor efficiency, turbine power, and the stator and volute total-pressure loss coefficients Y are summarized in Tab. 4. All simulation models show an agreement within 1% for all parameters except the total pressure loss coefficients of the volute and the stator. The losses in the volute, although of small magnitude, are increased by using the transition model. A noticeable difference can be observed in the stator, where the transition model decreases predicted losses by around 11%, possibly caused by laminar flow due to a low flow velocity upstream of the nozzle throat.

Table 4 Comparison of simulation models

Variation	Mass flow rate	Power	η_{ts}	$\eta_{\mathrm{rotor},ts}$	Y_{volute}	Y_{stator}
Transitional mixing plane	0.13215 kg/s	10231 W	0.8153	0.7966	$3.81 \cdot 10^{-5}$	0.2186
Fully turbulent full annulus	0.13207 kg/s	10275 W	0.8192	0.7909	$5.84 \cdot 10^{-5}$	0.2176
Transitional full annulus	0.13248 kg/s	10363 W	0.8238	0.7947	$6 \cdot 10^{-5}$	0.1931

Optimization setup

As this work aims to investigate the influence of the volute design on the ORC turbine design, an optimization workflow is developed to efficiently explore the design space. The optimization parameters are chosen as eight volute cross-sectional radii in 45° increments and the clocking angle between the volute and the stator. The lower and upper limits of the radii are based on the generability of the CAD model, while the limits for the clocking angle allow every possible relative position of volute tongue and stator leading edge. The limits of the optimization parameters are summarized in Tab. 5.

Table 5 Optimization parameter limits

Parameter	r_{45}	r_{90}	r_{135}	r_{180}	r_{225}	r_{270}	r_{315}	r_{360}	Clocking angle
Lower limit	1.5	1.6	1.7	1.8	1.9	5.5	5.6	5.7	0 °
Upper limit	6.5	16.5	17	17.5	18	18.5	19	19.5	15°

To achieve maximum turbine performance, it was decided to optimize for turbine power. Since the turbine is choked, the power is mostly proportional to the turbine efficiency, but includes additional possible blockage effects due to the position of the volute tongue.

As it is common practice in turbomachinery optimization, see e.g., (Schulz et al., 2025), and given the large number of parameters, a genetic optimization algorithm is chosen. It is based on genetics and the principle of natural selection, and belongs to the class of gradient-free evolutionary algorithms (Goldberg, 1989). The setup of the genetic algorithm is given in Tab. 6. The population size is set to five times the number of parameters, following the recommendation in Heinrich (2016). The function tolerance, which is the convergence criterion, is set to 0.001 between generations.

Table 6 Genetic algorithm setup

Parameter	**Value**
Population size	45
Mutation rate	0.1
Elite fraction	0.1
Crossover rate	0.8
Function tolerance	0.001

Using this algorithm setup, the optimization is conducted in MATLAB. MATLAB then hands over the parameters to Ansys CFX for meshing and simulation. The simulation is performed using the setup consisting of the volute, the full-annulus stator, and a singular rotor passage, and the design point (compare Tab. 3). Convergence is checked using the standard deviation of the turbine efficiency over the last 100 iterations, and the simulation is stopped if it drops below 0.00001. For each individual, the turbine power, turbine efficiency, total pressure loss coefficients of volute and stator, and mass flow and pressure loss variation per stator passage (mean μ and standard deviation σ) are extracted.

RESULTS

Optimization outcomes

During the optimization, a total of 750 individual geometries were evaluated before the algorithm converged. To gain a better understanding of the influence of the individual components and volute and stator on the turbine performance, Fig. 5 shows the turbine power in dependence on the total pressure losses per component. These are defined as:

$$Y = \frac{\Delta p_t}{p_{t,\mathrm{in}} - p_{\mathrm{in}}} \tag{4}$$

The figure clearly highlights that higher-power solutions do not necessarily correspond to minimum volute losses, as the vast majority of the total pressure loss occurs across the stator. Therefore, the design of the volute should be driven mainly by its effect on the stator, as opposed to a minimization of total pressure losses in the volute itself, which are negligible.

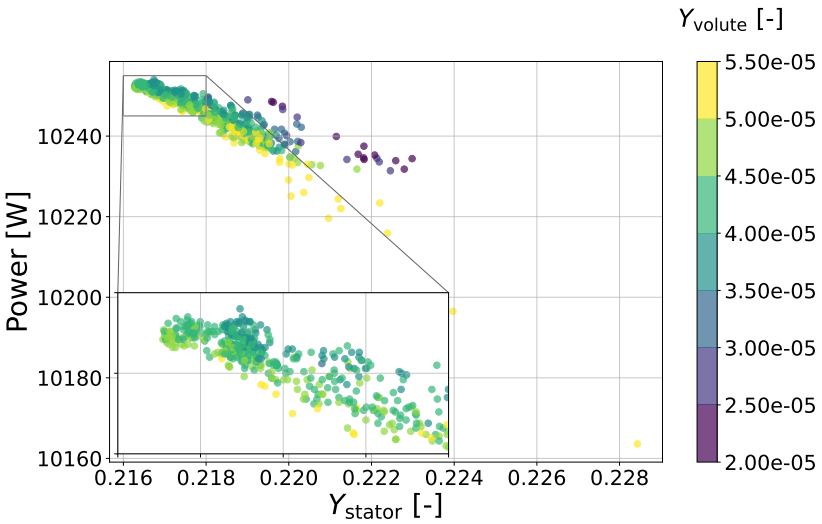


Figure 5 Loss coefficients across the stator/volute vs. turbine power

The mass flow rates and mass-averaged total pressure losses across each stator channel were also extracted during the optimization, and the individuals were compared using the coefficient of variation σ/μ in order to normalize the variations with respect to an average value, and are reported in Fig. 6. The mean value μ represents the average value of mass flow rate and loss coefficients across all blade channels, respectively, while the standard deviation represents how much that quantity varies between stator channels. Due to the stator being choked, there is relatively little variation in the mass flow rate, given on the left side. Instead, looking at the trends of total pressure loss, as shown on the right side, higher turbine power corresponds with more uniform total pressure losses across different passages.

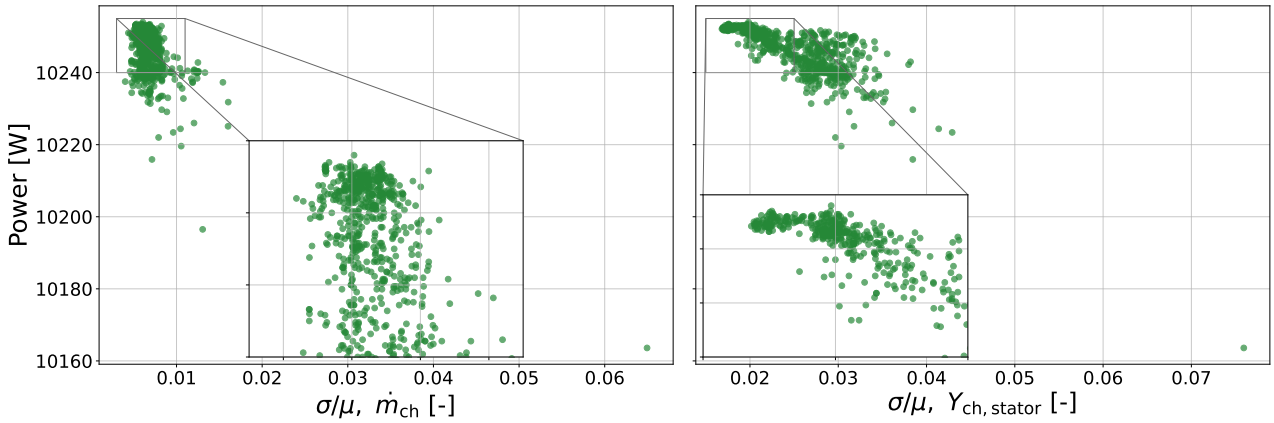


Figure 6 Variation of mass flow/loss coefficients across stator channels versus turbine power

The area distribution of the optimized volute in comparison to the baseline and the conventional design methods is shown in Fig. 7. It can be seen that the baseline design comprises a drastically bigger passage area than the conventional design methods. The optimal design starts relatively close to the conventional design methods (between 0 and 2 rad) and increases non-linearly afterwards. The largest passage area is close to the baseline design, likely caused by the constraint of the large volute inlet, which results from the fixed diameter of the connection to the test bench.

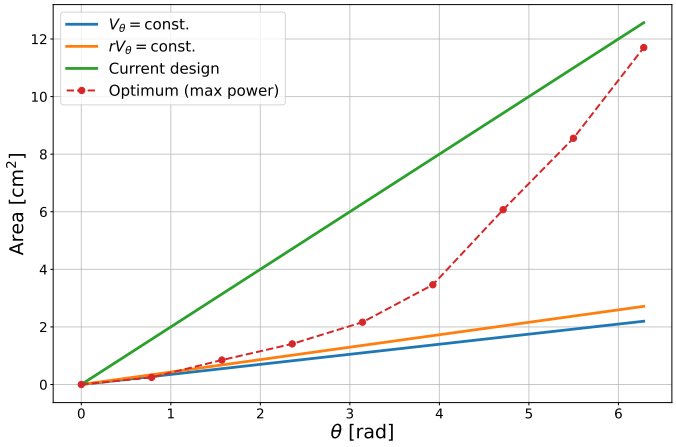


Figure 7 Passage area distribution, comparison of conventional design, manufactured volute (current design), and optimum passage area distribution

Performance map results

To investigate the influence of the different volute designs on turbine performance in off- and on-design conditions, the operating point matrix given in Tab. 3 was simulated for the optimized, baseline, constant tangential velocity, and free vortex volute using the full-annulus model. The results in terms of total-to-static efficiency for the different total inlet pressures are shown in Figs. 8, 9,10 and 11.

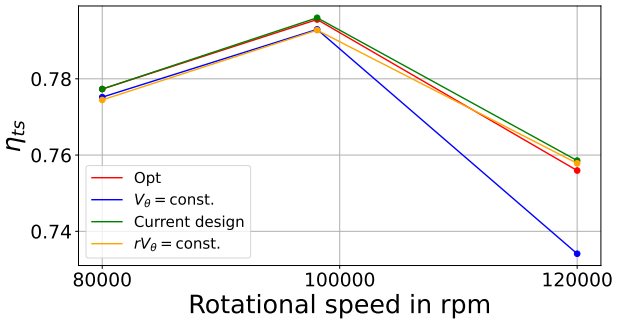


Figure 8 Isentropic total-to-static machine efficiency at $p_{t,\mathrm{in}} = 10.9\,\mathrm{bar}$

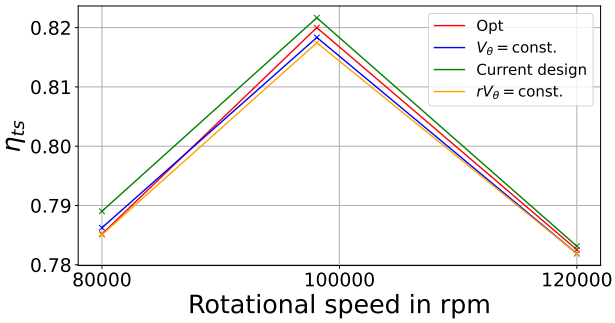


Figure 9 Isentropic total-to-static machine efficiency at $p_{t,\mathrm{in}} = 14.5\,\mathrm{bar}$

At an inlet pressure of 10.9 bar, the optimal (red) and the baseline design (green) achieve a nearly identical efficiency in OP1 and OP2, while in OP3, the baseline design performs better by around 0.3%pts. The free vortex design (orange) shows an efficiency reduction of around 0.3%pts. In OP1 and 2, the design of constant tangential velocity (blue) performs equally to the free vortex one, but shows a significant decrease in OP3.

When considering OP4, 5 and 6, the baseline design performs best, followed by the optimized with a decrease of around 0.2%pts, while the conventional design methods perform worst, showing a decrease of around 0.5%pts.

At the design total inlet pressure level of 18.1 bar, the optimized design outperforms the baseline one by about 0.5%pts. The free vortex design is the second best, showing a marginal decrease of around 01%pts. The constant tangential velocity design again performs the worst. When looking at the highest total inlet pressure, again, the optimized design is the best one, closely followed by the conventional design methods.

To show how the different volute designs affect the individual components, the total pressure loss coefficients of the volute and the stator, as well as the rotor total-to-static efficiency, are evaluated. The results for the design total inlet pressure are given in the following, while the ones for the other operating conditions are presented in Appendix . The volute losses, shown in Fig. 12, are negligible. However, the stator losses, given in Fig. 13, are influenced greatly by the volute design. The optimized volute results in the lowest stator losses, and when compared to the baseline, they are decreased by up to 6%. It is also evident that the stator losses are always lower with a lower rotor rotational speed.

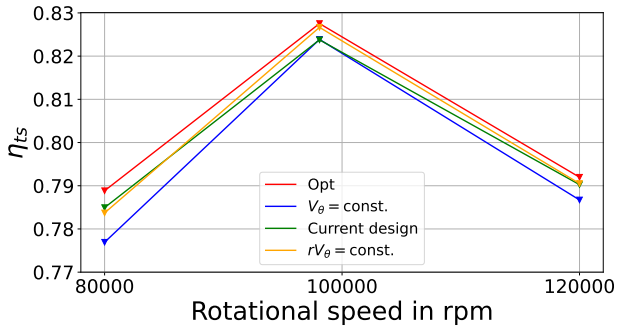


Figure 10 Isentropic total-to-static machine efficiency at $p_{t,\text{in}} = 18.1\,\text{bar}$

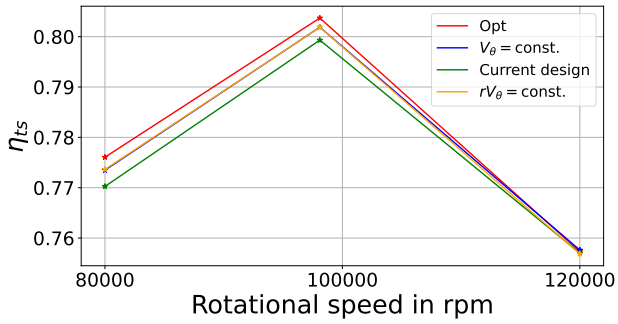


Figure 11 Isentropic total-to-static machine efficiency at $p_{t,\text{in}} = 23.5\,\text{bar}$

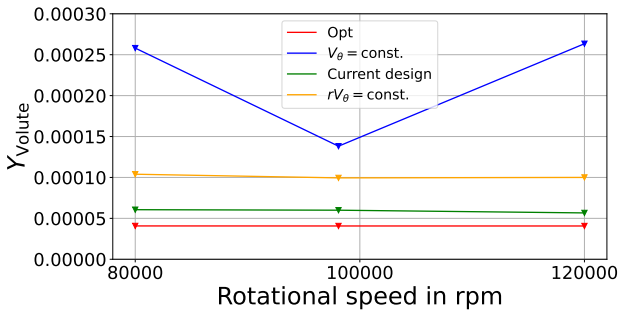


Figure 12 Volute total pressure loss coefficient at $p_{t,\text{in}} = 18.1\,\text{bar}$

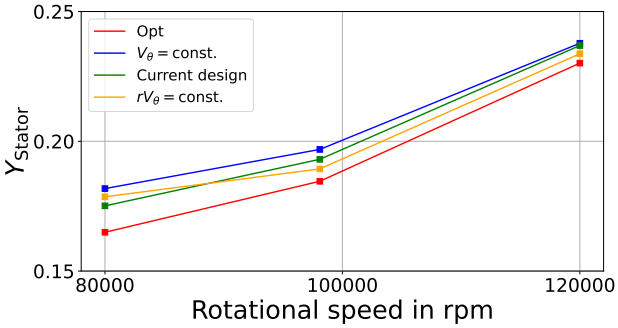


Figure 13 Stator total pressure loss coefficient at $p_{t,\text{in}} = 18.1\,\text{bar}$

The rotor total-to-static efficiency, which is illustrated in Fig. 14, shows variations of around 0.4%pts. between the best and the worst performing volute over the whole operating range. When comparing component efficiencies and machine efficiency, it can be concluded that the volute design mainly influences the stator total pressure loss, while the influence on the rotor is very limited.

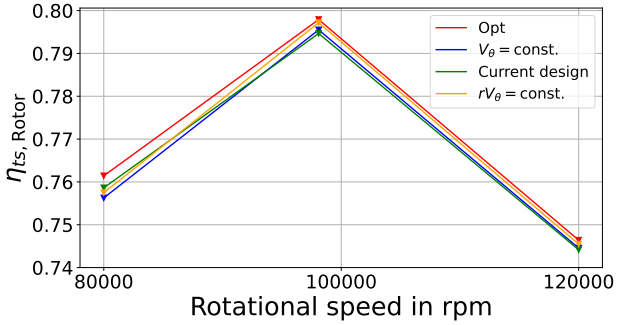


Figure 14 Isentropic total-to-static rotor efficiency at $p_{t,\text{in}} = 18.1\,\text{bar}$

The turbine power is depicted in Fig. 15. It is relatively similar for the two lower total inlet pressures. The highest variation of around 100 W is observed for OP9. Again, the conventional design method of constant tangential velocity performs the worst. As the mass flow rates are equal for the different designs due to choked flow, a comparison of this parameter is omitted.

When comparing total-to-static efficiencies and stator losses across the operating points, the free vortex design shows comparable performance to the optimized and baseline designs, while being significantly more compact. On the contrary, the constant-tangential-velocity design consistently underperforms compared to all other designs across the operating range. These observations lead to the recommendation of the free vortex design method as the preferred one, due to its simplicity, compactness, and comparable performance to the optimized design.

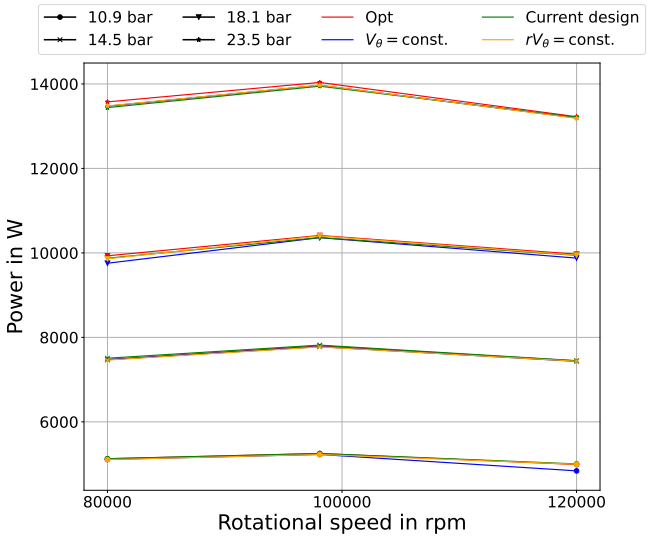


Figure 15 Turbine power

Design point results

To gain further insight into the mechanism behind the performance gain at DP conditions, the design point was evaluated in more detail. The mass flow-averaged velocity distribution over the circumference of the volute, normalized by the mass flow-averaged velocity at the volute inlet of 1.264 m/s, is displayed in Fig. 16. The conventional design methods achieve a nearly constant velocity apart from the tongue region (close to 0 rad), where the flow is accelerated. When looking at the optimized volute, which performs best, a large variation is observed, which is linked to the larger variation in passage area. The velocity magnitude is also decreased.

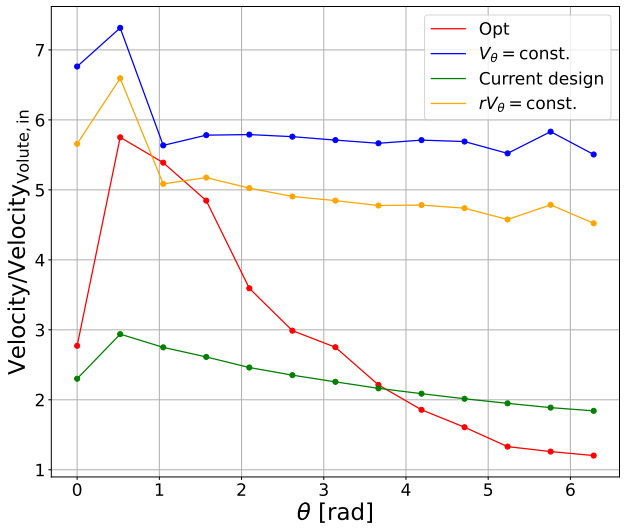


Figure 16 Volute velocity distribution at design point conditions

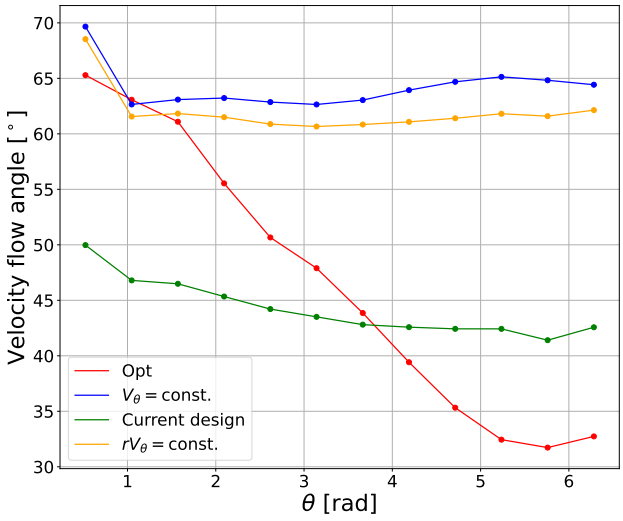


Figure 17 Flow angle distribution at design point conditions

Similarly, the mass flow-averaged velocity flow angle distribution at the stator inlet is presented in Fig. 17. Again, the conventional design methods achieve a nearly constant stator inflow, which nearly matches the metal angle of 63° perfectly, while the optimized design shows a large variation. However, the optimized volute performs better. This can partly be explained by the large leading edge radius of the stator vanes, which makes it insensitive to incidence.

The transition factors, which are equivalent to the γ of the transition model, in the stators of the different setups at the design point are depicted in Figs. 18, 19, 20 and 21. According to the documentation (Ansys, 2024*b*), ANSYS CFX uses a threshold of 0.02 for laminar flow. It shows that the volute design influences the position of the laminar-turbulent transition. The suction sides of the stator vanes upstream of the throat always stay laminar, while the vane passages are always turbulent downstream of the throat. When examining the pressure sides upstream of the throat, differences are observed. It shows that in the case of the constant tangential velocity and the free vortex design, the flow has already turned turbulent due to the

higher flow velocity, while the flow stays laminar in all but two stator passages for the baseline and the optimized design. The turbulence in the two passages is caused by the volute tongue.

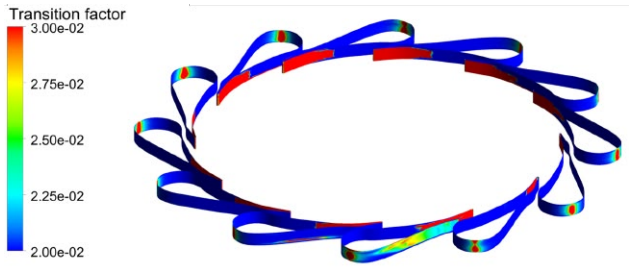


Figure 18 Laminar-turbulent transition in the stator of the baseline volute at the design point

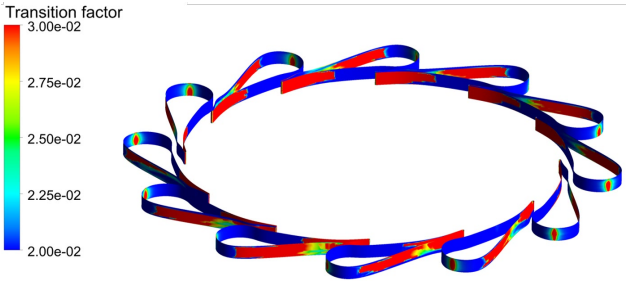


Figure 19 Laminar-turbulent transition in the stator of the constant tangential velocity volute at the design point

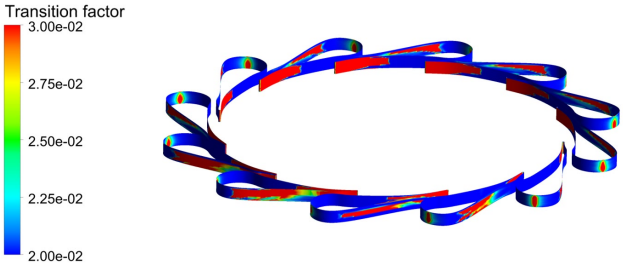


Figure 20 Laminar-turbulent transition in the stator of the free vortex volute at the design point

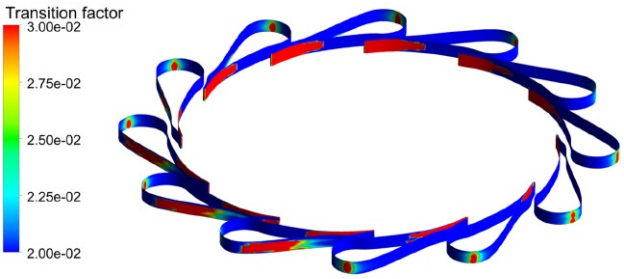


Figure 21 Laminar-turbulent transition in the stator of the optimized volute at the design point

The distribution of the turbulence kinetic energy (TKE) around the volute tongue and an iso-line indicating a velocity of 2 m/s, indicating the extent of the wake, at the design point of the optimized design is given in Fig. 22. It is evident that the best clocking position, as determined by the optimization, results in a wake position that coincides with the leading edge of the downstream stator. It is also observed that the wake does not follow the shape of the volute, but rather is deflected nearly centripetally. When compared to the wake of the baseline volute in Fig. 23, this deflection is weakened, while the wake follows the shape of the tongue for the free vortex (Fig. 24) and the constant tangential velocity design (Fig. 25). This is attributed to the lower flow velocity in the optimized volute. It can also be seen that the higher velocity in the conventionally designed volutes leads to a more turbulent wake, which mixes out faster and consequently is smaller.

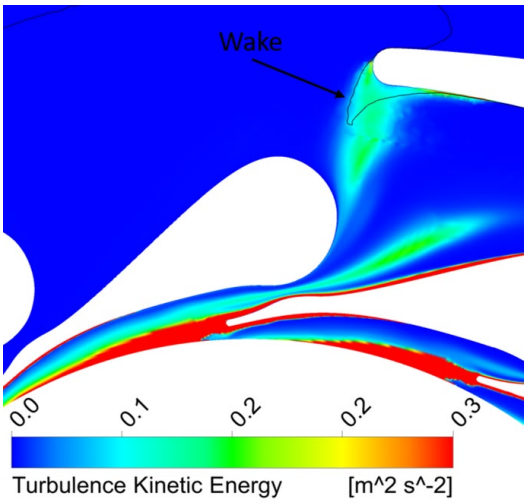


Figure 22 TKE distribution around the optimized volute tongue at DP

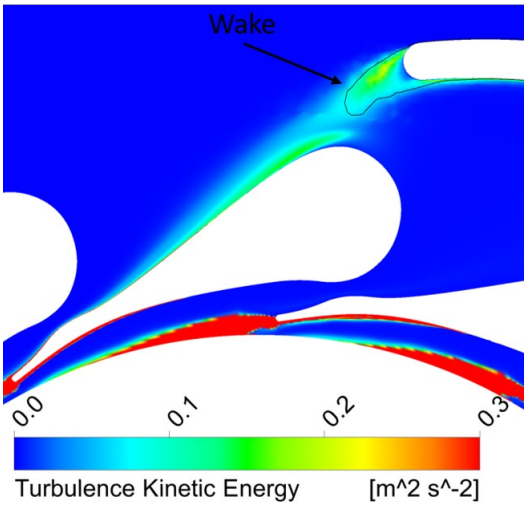


Figure 23 TKE distribution around the baseline volute tongue at DP

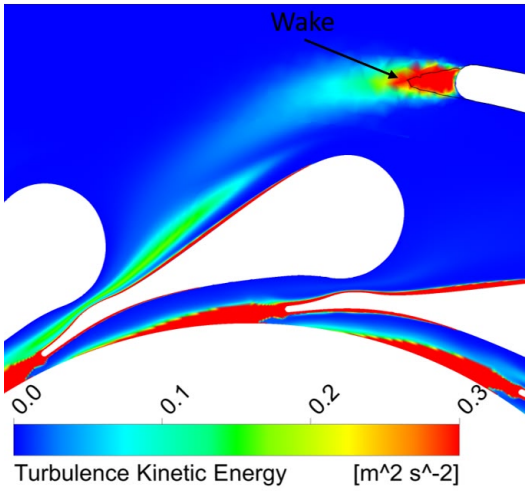


Figure 24 TKE distribution around the free vortex volute tongue at DP

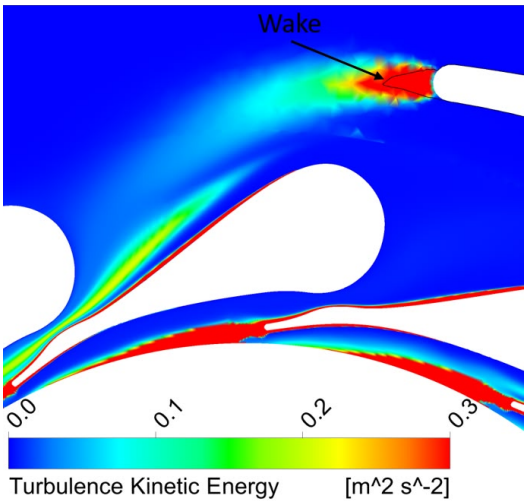


Figure 25 TKE distribution around the constant tangential velocity volute tongue at DP

CONCLUSIONS & OUTLOOK

In this work, the area distribution of the volute of a supersonic radial ORC turbine was optimized using CFD-based genetic optimization. Afterwards, the optimized design was compared to the baseline and two conventional design methods in on- and off-design conditions by means of full-annulus CFD. The main findings are as follows:

- The single-passage mixing plane setup achieved a surprisingly good agreement with the full annulus simulation, within 0.2%pts of isentropic efficiency. Therefore, such a model can be utilized in the initial design phase of ORC turbines.
- The use of the $\gamma - \mathrm{Re}_\theta$ transition model results in an increase in predicted performance of 0.5%pts, highlighting the influence of transition in ORC turbines.
- The optimization showed a potential of up to 0.5%pts in total-to-static isentropic turbine efficiency.
- Volute total pressure losses are negligible; however, the volute outflow leads to a significant variation in the stator total pressure losses.
- Stator performance is the main driver of the volute design.
- A more uniform volute outflow does not necessarily result in better turbine performance. In the case of ORC turbines, high densities in the volute correspond to lower flow velocities, which can lead to a partial laminar flow in the stator, thus increasing performance.
- The free vortex design method provides good performance for a wide range of operating conditions. It is therefore advisable to use this method for the design of ORC turbine volutes.

Although the findings reported in the article are limited to an optimization for a specific machine, they can inform designers about the importance of accounting for volute-stator interaction during detailed design. The outcome of the CFD-based volute optimization on machine performance gives information on what improvements designers can expect from such a procedure, and can thus inform a trade-off between computational resources and end-product performance.

The next steps are the commissioning and consequent experimental testing of the manufactured machine. Following this, the full-annulus simulations of the turbine stage conducted in this work will be compared to experimental data to validate the turbulence model selection. Additionally, it is planned to perform unsteady CFD analysis of the full-annulus turbine.

ACKNOWLEDGMENTS

We would like to acknowledge the funding by the Deutsche Forschungsgemeinschaft (DFG, German Research Foundation) under Germany's Excellence Strategy EXC 2163/1 Sustainable and Energy Efficient Aviation Project ID 390881007. We also thank the Leibniz Universität Hannover IT Services (LUIS) for providing the computational resources.

NOMENCLATURE

Acronyms

CFD	Computational fluid dynamics
ORC	Organic Ranking Cycle
Organic Rankine Cycle Hybrid Integrated Device	ORCHID
EERE	Extrapolated estimated relative error
GCI	Grid convergence index
MM	hexamethyldisiloxane
RANS	Reynolds-averaged Navier-Stokes
TKE	Turbulence kinetic energy

Roman symbols

M	Mach number [m/s]
Q	Volumetric massflow rate [m^3/s]
R	Volute cross-section radius [m]
U	Peripheral velocity [m/s]
V	Absolute flow velocity [m/s]
W	Relative flow velocity [m/s]
a	Speed of sound [m/s]
h	Specific enthalpy [J/kg]
i	Flow incidence angle [rad]
p	Pressure [Pa]
r	Radial coordinate [m]
s	Specific entropy [J/(kg·K)]
z	Axial coordinate [m]

Greek symbols

α	Absolute flow angle [°]
β	Relative flow angle [°]
β_g	Blade geometrical angle [°]
δ	Flow deviation angle [°]
η	Efficiency
ϕ	Meridional angle[rad]
γ	Ratio of specific heats [-]
ρ	Density [kg/m^3]

Subscripts

0	Volute inlet
1	Stator inlet/volute outlet
2	Stator outlet/rotor inlet
3	Rotor outlet
in	Component inlet
θ	Tangential velocity component
r	Radial velocity component
s	Static quantity
t	Total quantity
r,t	Relative total quantity

References

Agreement, P. (2015), Paris agreement, *in* 'Report of the Conference of the Parties to the United Nations Framework Convention on Climate Change (21st Session, 2015: Paris).', Vol. 4, HeinOnline, p. 2017.

ANSYS (2024*a*), 'Ansys cfx solver theory guide', *Release 2024.2* .

Ansys (2024*b*), 'How to visualize the laminar and turbulent regimes in a transitional simulation in ansys cfx', https://innovationspace.ansys.com/courses/wp-content/uploads/sites/5/2024/01/Tidbits-Turbulence-CFX-Lesson-5.pdf. Online; accessed 16 April 2026.

Beltrame, F., Head, A. J., De Servi, C., Pini, M., Schrijer, F. and Colonna, P. (2021), First experiments and commissioning of the orchid nozzle test section, *in* 'Proceedings of the 3rd International Seminar on Non-Ideal Compressible Fluid Dynamics for Propulsion and Power', Springer International Publishing, p. 169–178.
URL: *http://dx.doi.org/10.1007/978-3-030-69306-0_18*

Chung, T. H., Ajlan, M., Lee, L. L. and Starling, K. E. (1988), 'Generalized multiparameter correlation for nonpolar and polar fluid transport properties', *Industrial & engineering chemistry research* **27**(4), 671–679.

Colonna, P., Van Der Stelt, T. and Guardone, A. (2004), 'Fluidprop (version 3.0): A program for the estimation of thermophysical properties of fluids', *A computer program since* .

Cullen, J. M. and Allwood, J. M. (2010), 'Theoretical efficiency limits for energy conversion devices', *Energy* **35**(5), 2059–2069.

De Servi, C. M., Burigana, M., Pini, M. and Colonna, P. (2019), 'Design method and performance prediction for radial-inflow turbines of high-temperature mini-organic rankine cycle power systems', *Journal of Engineering for Gas Turbines and Power* **141**(9), 091021.

Ebaid, M., Bhinder, F. and Khdairi, G. (2003), 'A unified approach for designing a radial flow gas turbine', *J. Turbomach.* **125**(3), 598–606.

Filali, A. and Semmari, H. (2025), Designing a radial turbine for orc system: effect of the organic fluid, *in* '2025 3rd International Conference on Electronics, Energy and Measurement (IC2EM)', IEEE, pp. 1–6.

Fister, W. (1986), *Fluidenergiemaschinen*, Springer Berlin Heidelberg.
URL: *http://dx.doi.org/10.1007/978-3-642-82524-8*

Goldberg, D. E. (1989), 'Genetic algorithms in search, optimization and machine learning', *Reading MA* .

Head, A. (2021), Novel Experiments for the Investigation of Non-Ideal Compressible Fluid Dynamics, PhD thesis, Delft University of Technology, Faculty of Aerospace Engineering, Flight Performance & Propulsion.

Heinrich, M. (2016), 'Genetic optimization of turbomachinery components using the volute of a transonic centrifugal compressor as a case study'.

Kato, K. (1993), The modeling of turbulent flow around stationary and vibrating square cylinders, *in* 'Proc. of 9th Symp. Turbulent Shear Flows', pp. 1041–1046.

Majer, M. (2025), Supersonic organic Rankine cycle radial-inflow turbines for onboard thermal energy harvesting: Preliminary design guidelines and detailed design of a laboratory test rig for experimental validation, PhD thesis, Delft University of Technology, Faculty of Aerospace Engineering, Flight Performance & Propulsion.

Majer, M., Chatterton, S., Dassi, L., Gheller, E., Pennacchi, P. E. L. M., Colonna, P. and Pini, M. (2025), 'Mechanical design and rotordynamic analysis of the orchid turbine', *Journal of the Global Power and Propulsion Society* **9**(May), 45–66.
URL: *http://dx.doi.org/10.33737/jgpps/195567*

Menter, F. R., Kuntz, M. and Langtry, R. (2003), 'Ten years of industrial experience with the sst turbulence model', *Turbulence, heat and mass transfer* **4**(1), 625–632.

Menter, F. R., Langtry, R. B., Likki, S., Suzen, Y., Huang, P. and Völker, S. (2006), 'A correlation-based transition model using local variables—part i: model formulation', *Journal of turbomachinery* **128**(3), 413–422.

Michelis, T., Head, A. J., Majer, M., Colonna, P. and De Servi, C. (2024), 'Assessment of particle image velocimetry applied to high-speed organic vapor flows', *Experiments in Fluids* **65**(6).
URL: *http://dx.doi.org/10.1007/s00348-024-03822-z*

Oliveti, M., Wheeler, A. P. and Persico, G. (2020), Direct simulations of non-ideal supersonic flows in the trailing edge region, *in* 'International Seminar on Non-Ideal Compressible-Fluid Dynamics for Propulsion & Power', Springer, pp. 81–95.

Pethurajan, V., Sivan, S. and Joy, G. C. (2018), 'Issues, comparisons, turbine selections and applications–an overview in organic rankine cycle', *Energy conversion and management* **166**, 474–488.

Qiang, X., Teng, J. and Du, Z. (2010), 'Influence of various volute designs on volute overall performance', *Journal of thermal science* **19**(6), 505–513.

Rahbar, K., Mahmoud, S., Al-Dadah, R. K., Moazami, N. and Mirhadizadeh, S. A. (2017), 'Review of organic rankine cycle for small-scale applications', *Energy conversion and management* **134**, 135–155.

Roache, P. J. (1998), *Verification and validation in computational science and engineering*, Vol. 895, Hermosa Albuquerque, NM.

Schulz, Y., Kuestner, C., Kohl, J. M. and Mimic, D. (2025), Variable amplitude leading edge tubercle optimization of rotor 37, *in* '16th European Turbomachinery Conference (ETC16)'.

Seume, J. R., Peters, M. and Kunte, H. (2017), Design and test of a 10kw orc supersonic turbine generator, *in* 'Journal of Physics: Conference Series', Vol. 821, IOP Publishing, p. 012023.

Shah, S. P., Channiwala, S., Kulshreshtha, D. and Chaudhari, G. (2014), 'Design and numerical simulation of radial inflow turbine volute.', *International Journal of Turbo & Jet-Engines* **31**(4).

Span, R. and Wagner, W. (2003), 'Equations of state for technical applications. i. simultaneously optimized functional forms for nonpolar and polar fluids', *International journal of thermophysics* **24**(1), 1–39.

Stepanoff, A. J. (1957), *Radial- und Axialpumpen: Theorie, Entwurf, Anwendung*, Springer Berlin Heidelberg.
URL: *http://dx.doi.org/10.1007/978-3-662-25101-0*

Suhrmann, J. F., Peitsch, D., Gugau, M. and Heuer, T. (2012), On the effect of volute tongue design on radial turbine performance, *in* 'Turbo Expo: Power for Land, Sea, and Air', Vol. 44748, American Society of Mechanical Engineers, pp. 891–901.

APPENDIX A - Component performance

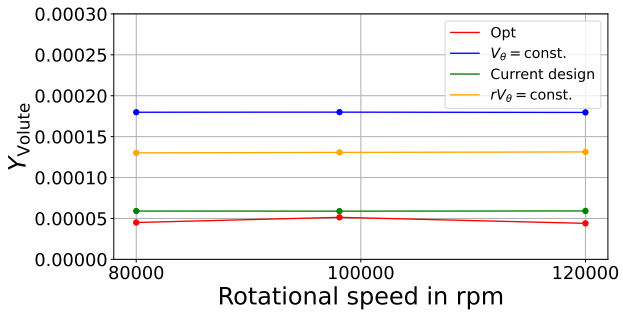


Figure 26 Volute total pressure loss coefficient at $p_{t,\text{in}} = 10.9\,\text{bar}$

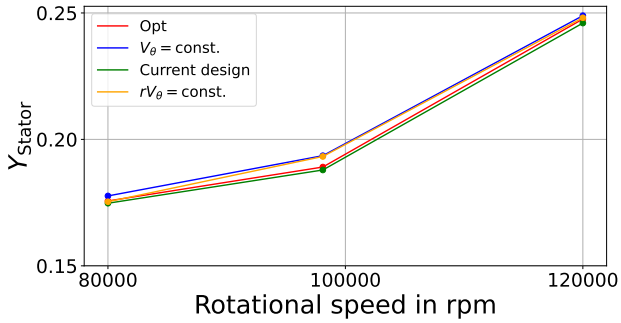


Figure 27 Stator total pressure loss coefficient at $p_{t,\text{in}} = 10.9\,\text{bar}$

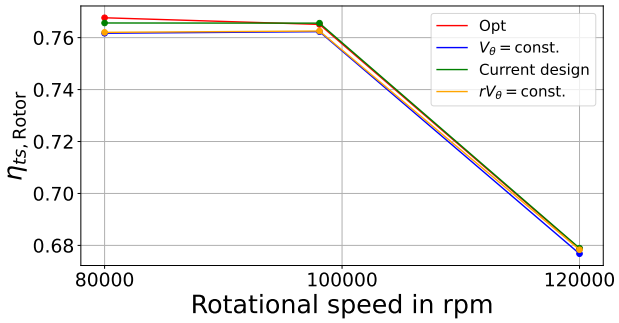


Figure 28 Isentropic total-to-static rotor efficiency at $p_{t,\text{in}} = 10.9\,\text{bar}$

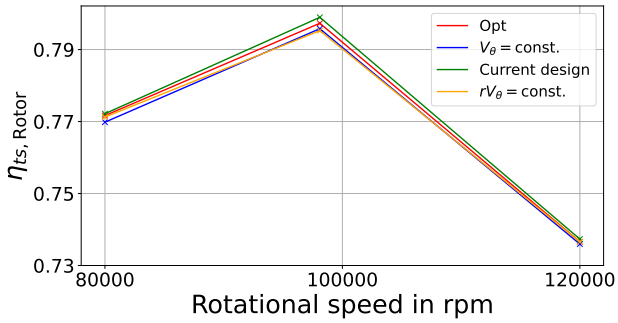


Figure 29 Isentropic total-to-static rotor efficiency at $p_{t,\text{in}} = 14.5\,\text{bar}$

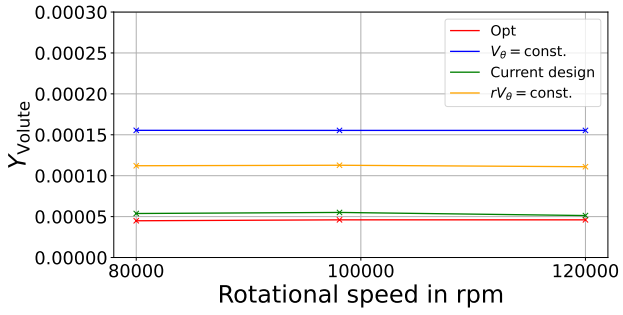


Figure 30 Volute total pressure loss coefficient at $p_{t,\text{in}} = 14.5\,\text{bar}$

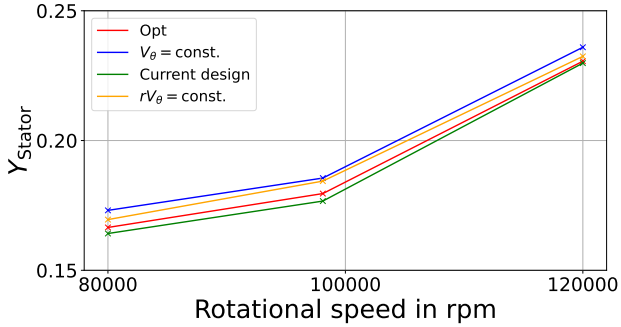


Figure 31 Stator total pressure loss coefficient at $p_{t,\text{in}} = 14.5\,\text{bar}$

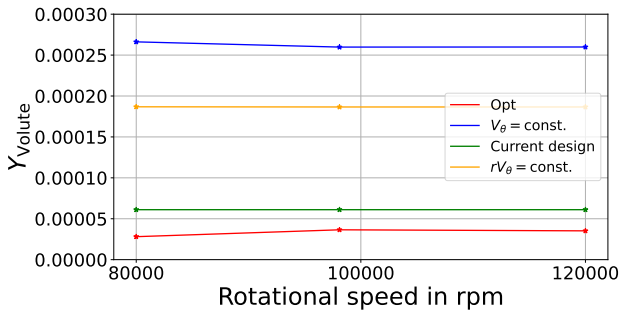


Figure 32 Volute total pressure loss coefficient at $p_{t,\text{in}} = 23.5\,\text{bar}$

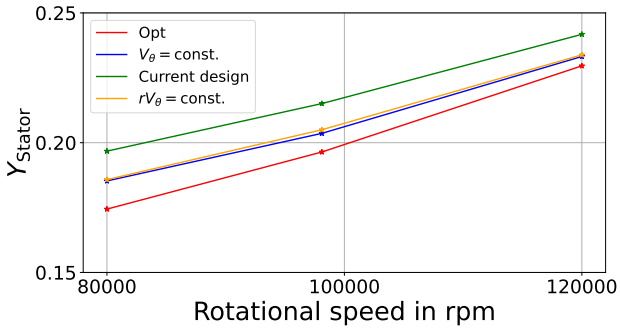


Figure 33 Stator total pressure loss coefficient at $p_{t,\text{in}} = 23.5\,\text{bar}$

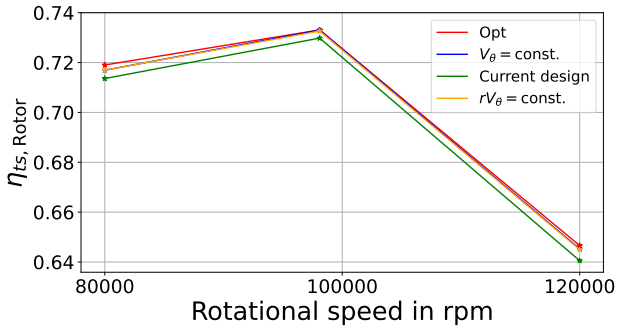


Figure 34 Isentropic total-to-static rotor efficiency at $p_{t,\text{in}} = 23.5\,\text{bar}$